Journal of Alloys and Compounds 488 (2009) 459–464

Contents lists available at ScienceDirect

Journal of Alloys and Compounds

journal homepage: www.elsevier.com/locate/jallcom

Investigation of structural, electrical and magnetic properties of $BiFeO_3$–$Bi(MgTi)O_3$–$PbTiO_3$ ceramic system

Radheshyam Rai[a,*], Andrei Kholkin[a], Shyamakant Pandey[b], N.K. Singh[b]

[a] Department of Ceramics and Glass Engineering and CICECO, University of Aveiro, 3810-193 Aveiro, Portugal
[b] Department of Physics, V. K .S. University, Ara 802301, India

ARTICLE INFO

Article history:
Received 7 July 2009
Received in revised form 2 September 2009
Accepted 3 September 2009
Available online 10 September 2009

Keywords:
Powders
Solid-state reaction
Grain size
Dielectric properties
Electrical conductivity

ABSTRACT

$[(BiFeO_3)_y(BiMg_{0.5}Ti_{0.5}O_3)_{1-y}]_x[PbTiO_3]_{1-x}$ (BF–BMT–PT) ceramic powders were prepared by high temperature solid-state reaction method. X-ray diffraction analysis of the powders suggests the formation of a single-phase material with tetragonal structure. SEM images exhibit the uniform distribution of grains. Polarization vs electric field (*P*–*E*) hysteresis studies show maximum remanent polarization ($P_r \sim 14\ \mu C/cm^2$) for composition $X = 0.65$. Dielectric studies of the compounds as a function of temperature (from RT to 550 °C) (test frequency 100 kHz) show that the compounds undergo a diffuse phase transition with a transition temperature increasing with decreasing *X*. The diffusivity parameter of the phase transition for these compounds yielded values between 1.6 and 1.8 indicating significant variation of degree of disordering in the system.

1. Introduction

Perovskite solid solutions have been an active area of research due to importance in ferroelectric and piezoelectric applications and their fascinating physical properties [1–6]. In particular, Bi-based ferroelectrics are under intense investigation, because they exhibit both large polarization [7–9] and multiferroic behavior [10,11]. The advantages of bismuth perovskites over PZT are environmentally more friendly materials, a higher mechanical strength and Curie temperature. In this family of materials, BNT-based crystalline solutions are considered to be one of the best candidates for lead free or low-lead-content piezoelectric materials due to their strong ferroelectricity [12–14]. However, BNT-based ceramics are difficult to pole due to their large coercive field. Early studies on perovskite-structured $Bi(Me)O_3$–$PbTiO_3$ solid solutions were mostly concerned with compounds containing transition metal Me ions such as Fe^{3+} and Mn^{3+} [12,13]. $BiFeO_3$ is reported to exhibit eight structural phase transitions [15] characterized by antiferromagnetic ordering ($T_N = 397$ °C) and ferroelectric ordering ($T_c = 836$ °C) [10]. The ferroelectric phase in $BiFeO_3$ is stable up to 836 °C. But low resistivity of the samples at room temperature makes using its multiferroic properties very difficult. These materials show high temperature ferroelectric–paraelectric phase transitions but the piezoelectric and dielectric properties were limited or unknown due to their high electrical conductivity, which prevented poling of the ceramics. Recently, Eitel et al. [5,14] investigated more stable valence B-site cations in Bi-based perovskites and demonstrated that a material, $BiScO_3$–$PbTiO_3$ (BS–PT), has excellent piezoelectric coefficients (d_{33} – 500 pC/N). A recent transmission electron microscopy (TEM) investigation revealed that the FE domain structures and electron diffraction patterns in BS–PT were very similar to those in the $PbZrO_3$–$PbTiO_3$ (PZT) solid solution [16]. Eitel et al. [14] have proposed that as the tolerance factor for the rhombohedral or monoclinic end member decreases, keeping lead titanate as a tetragonal phase, the transition temperature at the MPB will raise.

It has been known that the most favorable piezoelectric properties are found at the morphotropic phase boundary (MPB) between the rhombohedral and tetragonal ferroelectric phases. In the ABO_3 structure, the valences of the A (12-cordinated) and B (6-cordinated) cations are usually 2^+ and 4^+, respectively, so a lot of perovskite materials were created with doping by other types of cations into the stoichiometry and/or introducing anion deficiency [10,11,17]. Sharma and Hall [18] and Sharma et al. [19] studied a new high temperature solid–solution system BMZ–PT. They studied the effect of addition of BF in BMZ–PT system on the structural and ferroelectric properties. Effect of BF on BMZ–PT is to decrease the spontaneous and residual polarization and increase the Curie temperature of the system. Rai et al. [20] reported that the BMT–PT ceramics exhibit many interesting features, such as structural change, shift in transition temperature with respect to different compositions.

* Corresponding author. Tel.: +351 962782932; fax: +351 234425300.
E-mail address: radheshyamrai@ua.pt (R. Rai).

0925-8388/$ – see front matter © 2009 Elsevier B.V. All rights reserved.
doi:10.1016/j.jallcom.2009.09.011

Here we study the ternary system ($[(BiFeO_3)_y(BiMg_{0.5}Ti_{0.5}O_3)_{1-y}]_x[PbTiO_3]_{1-x}$) aiming at the development of high dielectric constant multiferroic lie (magnetoelectric) materials. It must be noted that the introduction of BF to the binary perovskite BMT–PT creates a ternary system BF–BMT–PT which is also a perovskite (explained in section of X-ray diffractograms). In this paper, we investigated the structural, dielectric and electrical properties of the (BF–BMT–PT) ceramic system, aiming at maximizing its ferroelectric piezoelectric properties while maintaining the multiferroic coupling.

2. Experimental procedures

Polycrystalline samples of $[(BiFeO_3)_y(BiMg_{0.5}Ti_{0.5}O_3)_{1-y}]_x[PbTiO_3]_{1-x}$, where $Y = 0.25$, and/or $X = 0.45$, 0.55, 0.60, and 0.65, were synthesized from high purity oxides. Bi_2O_3, Fe_2O_3, TiO_2, MgO, and PbO (99.9% M/S Aldrich Chemicals) using high temperature solid-state reaction technique in an ambient atmosphere. The constituent compounds in suitable stoichiometry were thoroughly mixed in a ball milling unit for 24 h. The calcined fine powder was cold pressed into cylindrical pellets of 10 mm in diameter and 1–2 mm in thickness using a hydraulic press with a pressure of 6×10^7 kg m^{-2}. These pellets were sintered at 1050 °C for 4 h. The formation and quality of compounds were verified by X-ray diffraction (XRD) technique. The XRD pattern of the compounds was recorded at room temperature using X-ray powder diffractometer (Rigaku Minifiex, Japan) with CuKα radiation ($\lambda = 1.5418$ Å) in a wide range of Bragg angles 2θ ($20° \le 2\theta \le 60°$) at a scanning rate of 2° min^{-1}. SEM micrographs were acquired with the help of a JEM-2000FX (JEOL Ltd.) scanning electron microscope (operated at 20 keV). SEM photographs were taken from the fracture surface of the specimens. The dielectric constant (ε) and loss tangent ($\tan\delta$) of the compounds were measured using a 4192A LF Impedance Analyser (HP) as a function of frequency at room temperature [RT] and temperature (RT to 500 °C) at different frequencies with a home made experimental setup. Ferroelectric hysteresis was measured by using Radiant technologies, Precision High Voltage Interface Trek MODEL 609B at room temperature.

Table 1
Structural data for different compositions of BF–BMT–PT.

Sample	Structure	a	c	c/a	Measured density (g/cm^3)
$X = 0.45$	Tetragonal	3.5692	4.0200	1.12	7.33
$X = 0.55$	Tetragonal	3.5689	4.0302	1.12	7.35
$X = 0.60$	Tetragonal	3.5652	4.0542	1.13	7.55
$X = 0.65$	Tetragonal	3.5523	4.6106	1.29	7.68

3. Results and discussion

The narrow and symmetric diffraction peaks of the BF–BMT–PT compounds indicate homogeneity and good crystallization of the samples. The room temperature XRD patterns of the BF–BMT–PT perovskite type ceramics are plotted in Fig. 1. The X-ray analysis indicates that all the compounds were of tetragonal structure at room temperature. All the reflection peaks were indexed using observed inter-planar spacing d, and lattice parameters of BF–BMT–PT were determined using a least-squares refinement method. All the calculations were done using a computer program package Powdin [21]. A good agreement between calculated and observed d values of all diffraction lines (reflections) of BF–BMT–PT of different composition suggests that there is no change in the basic crystal structure. Some extra small peaks of $Bi_2FeO_{2.75}$ were also observed in the XRD patterns. Crystal tetragonality (c/a) (Table 1) is found to increase with increase in substitution content resulting in hard and dense ceramics. The tetragonality is increasing with increase in BF–BMT ratio (Fig. 1a) in the sample. There is

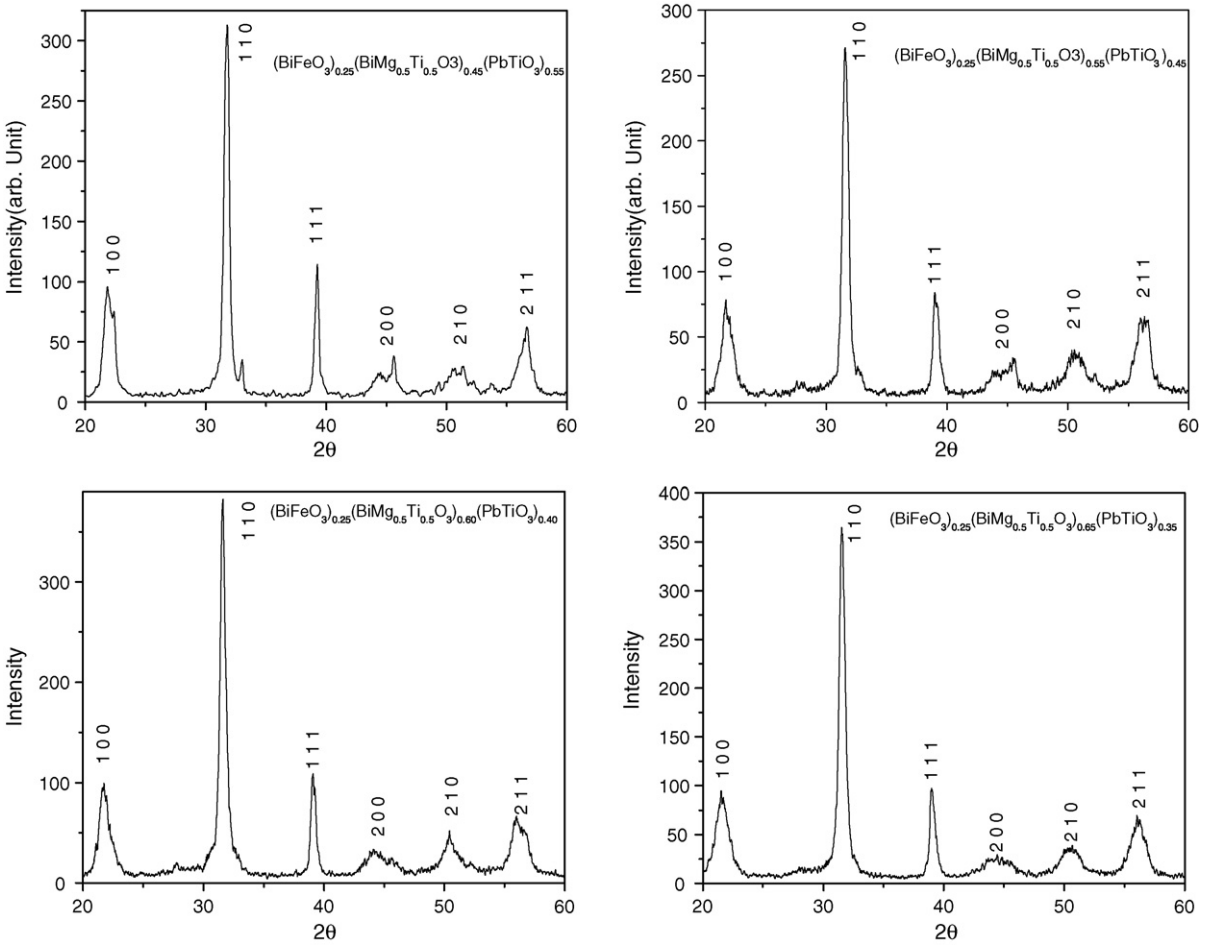

Fig. 1. X-ray powder diffraction patterns of the BF–BMT–PT ceramics for different compositions. (a) Plots of tetragonality vs concentration (mol%) of different compositions.

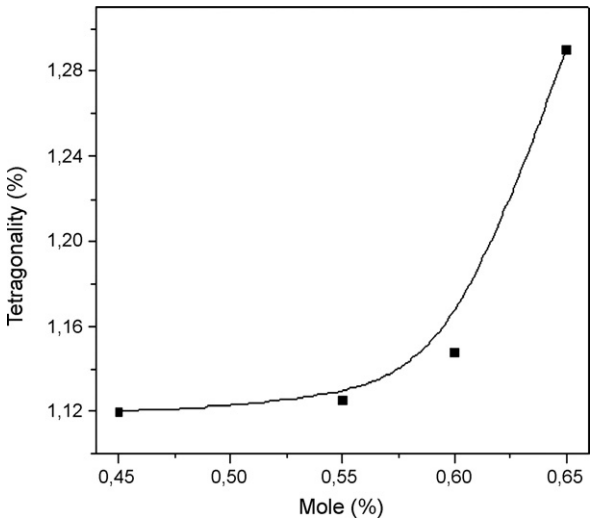

Fig. 1. (*Continued*).

1.12% tetragonality for 0.45 composition and it is increased to 1.29% for the $X = 0.65$. This confirms the hardening effect of the inclusion of BMT content in the BF–BMT–PT system. The microstructure of BF–BMT–PT ceramics was investigated by scanning electron microscope (SEM) with energy dispersive detector for X-rays (EDX). Our studies concentrated on the effect of optimal processing conditions on the final microstructure. SEM images of BF–BMT–PT with different content ratio are presented in Fig. 2 . The material with an average grain size of 10–15 nm was obtained. The fine-grained microstructure is quite uniform, with some internal and grain-boundary porosity. The influence of the thermal treatment conditions is very important in the formation of high-quality BF–BMT–PT ceramics. The most important factor influencing the size and homogeneity of grains is the sintering time. The total ther-

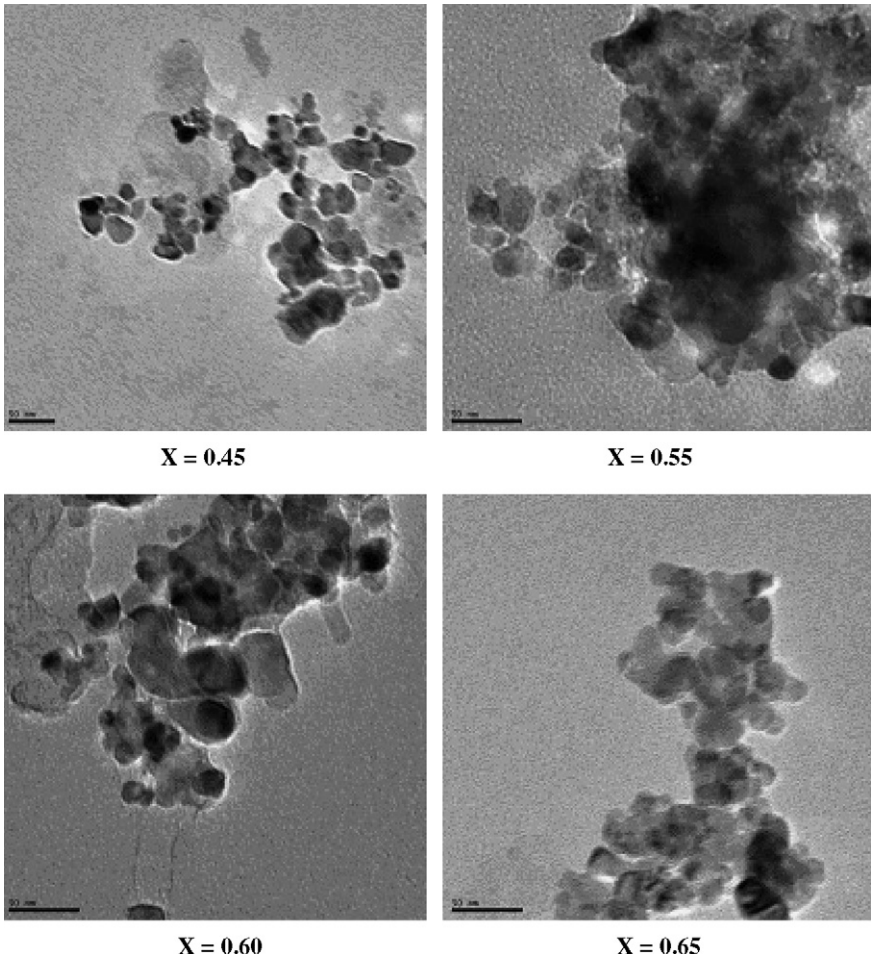

Fig. 2. SEM micrographs of polished surfaces for different BF–BMT–PT compositions.

mal budget for sintering process, promote the grain growth in the samples. EDX analysis of individual grains in different compositions indicates a homogeneous distribution of all the constituent elements in the ceramics.

Fig. 3 shows variation of ε with frequency at room temperature for all compositions. It was found that with the increase of frequency ε slowly decreases following the logarithmic law. This type of relaxation can be related to the domain wall propagation in a random media similar to that in magnetic systems. Damjanovic [22] observed direct piezoelectric effect in doped PZT ceramics and related it to Rayleigh type dependence. The same type of frequency dependence is found in many ferroelectric ceramics [23,24]. Room temperature variation of dielectric loss with frequency does not show an appreciable change. In our case, the observed increase in the dielectric permittivity vs composition X is attributed to the increased spontaneous polarization as the ferroelectrically active Ti ions goes to B-site cations of perovskite structure. The larger values of ε at room temperature and lower frequency dispersion in BF–BMT–PT may also be ascribed due to the interfacial and dipolar contribution of polarization [25]. Fig. 4a and b shows the variation of ε and $\tan\delta$ of BF–BMT–PT with temperature at 100 kHz frequency. Here, the dielectric permittivity increases gradually with an increase in temperature up to transition temperature (T_c) and then decreases. The region around the dielectric peak is apparently

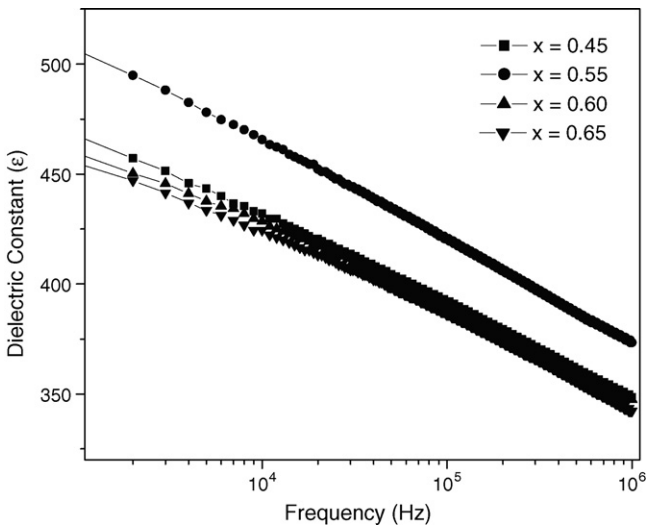

Fig. 3. Variation of dielectric constant of BF–BMT–PT as a function of frequency at room temperature.

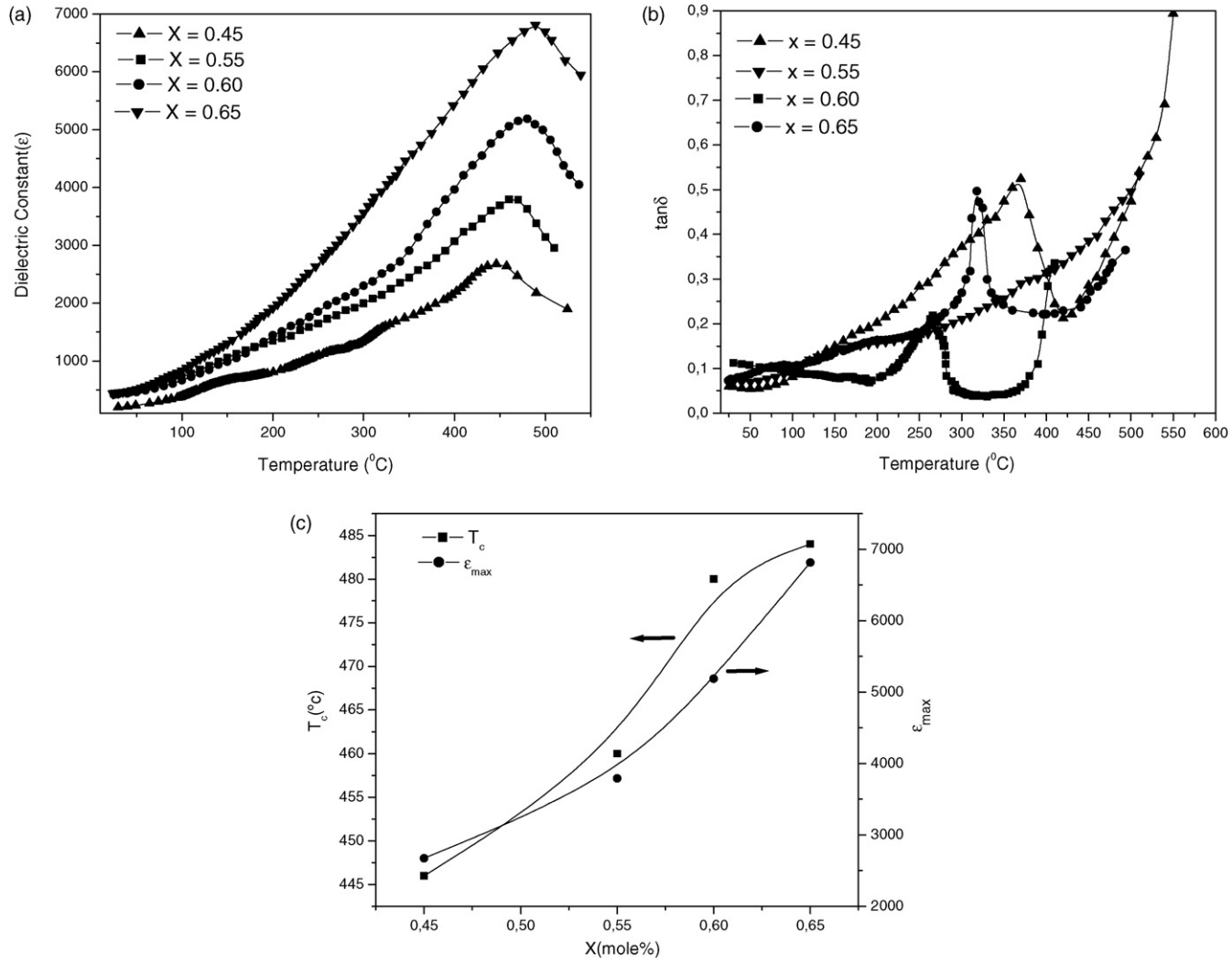

Fig. 4. (a) Variation of dielectric constant of BF–BMT–PT as a function of temperature at 100 kHz. (b) Variation of dielectric loss of BF–BMT–PT as a function of temperature at 100 kHz. (c) Dielectric constant maximum and transition temperatures vs doping concentration (mol%) at 100 kHz.

Table 2
Some physical parameters for different compositions of BF–BMT–PT.

Physical parameters	$X=0.45$	$X=0.55$	$X=0.60$	$X=0.65$
ε_{rt}	196	431	419	439
$\tan\delta_{rt}$	0.060	0.070	0.11	0.072
T_c	446	460	480	484
ε_{max}	2673	3793	5187	6816
$\tan\delta_{max}$	0.28	0.39	Out of limit	0.33
γ	1.60	1.70	1.75	1.8

broadened. The broadening or diffuseness of peak occurs mainly due to compositional fluctuation and/or substitution disordering in the arrangement of cations in one or more crystallographic sites of the BF–BMT–PT structure. The value of peak dielectric permittivity (ε_{max}) increases initially with the increase of concentration (Table 2). It reveals a maximum near to 484 °C. Above this temperature the permittivity does not appear to follow the Curie–Weiss law as required by thermodynamics. For the illustrative and comparative purpose, the plots of ε_{max} vs concentration at 100 kHz for various compositions are drawn in Fig. 4c. With the increase of BMT content, increase Curie temperature and dielectric constant in this ferroelectric system. Additionally, a maximum value in ε_{max} is found at 0.65 mol% BMT.

We have also made attempts to measure the induced polarization electric field (P–E) hysteresis loop at room temperature (Fig. 5). Well-saturated P–E loop could be observed for increasing E showing full domain switching. The $X=0.65$ shows the saturation in hysteresis loops. However, during measurement, application of higher fields was restricted due to sufficiently high conductivity of the samples. The observed coercive filed is $E_c \sim 70$ kV/cm and remanent polarization is $P_r \sim 14\ \mu C/cm^2$. Experiments are in progress to improve the density of the samples so as to reduce the conductivity. No saturation in polarization–electric field (P–E) curve could be obtained for first two ceramics compositions up to the maximum applied electric field due to their low resistivity. Unsaturated ferroelectric loops are common in bulk materials. Amongst the four studied compositions, BF–BMT–PT samples could not hold electric field beyond 70 kV/cm^2 and further increase in electric field leads to electric breakdown. This maximum limit is reduced to 20 kV/cm for first two samples of BF–BMT–PT. This could be explained on the basis of FE-SEM images. The last two samples ($X=0.60$, 0.65) have

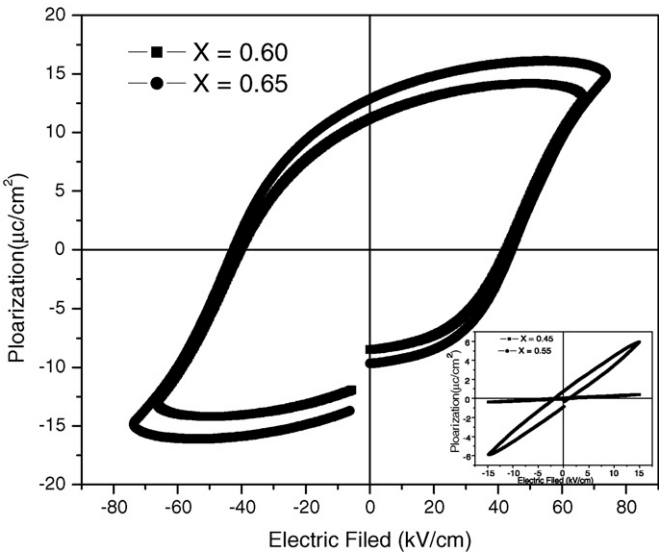

Fig. 5. P–E hystersis loops for BF–BMT–PT ceramics at room temperature.

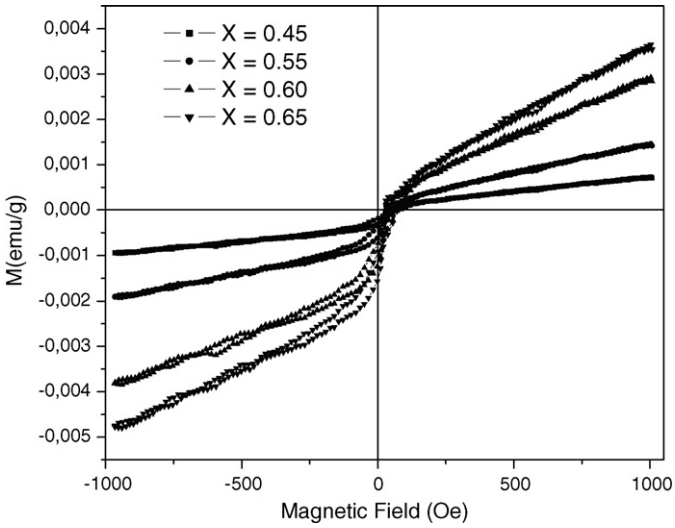

Fig. 6. Magnetization vs magnetic field curves for BF–BMT–PT samples at room temperature.

highly dense, uniformly distributed grains with nearly no pores and hence it shows high resistivity. The density of later two samples ($X=0.55$, 0.65) samples is 7.68 g/cm^3. The resistivity is reduced for first two samples ($X=0.45$, 0.55) which can be attributed to porous and underdeveloped grains with relatively less density, i.e. 7.35 g/cm^3.

In BF–BMT–PT, Fe magnetic moments are coupled ferromagnetically within the pseudo cubic (1 1 1) plane and antiferromagnetically between adjacent planes. There is a canting of antiferromagnetic sublattices resulting in a macroscopic magnetization. Superimposed on antiferromagnetic ordering, there is a spiral spin structure which leads to cancellation of macroscopic magnetization. Magnetization is induced in the sample whenever this spiral structure is suppressed [26]. All the samples show unsaturated magnetization loops (Fig. 6) which confirm the basic antiferromagnetic nature of the compounds. The magnetization increases with the increase in content of BF–BMT. The magnetization is higher, when the concentration of BF–BMT–PT is increased from 0.45 to 0.65. This could be due to the structural distortion in the perovskite, i.e., the canted spin arrangement of unpaired elec-

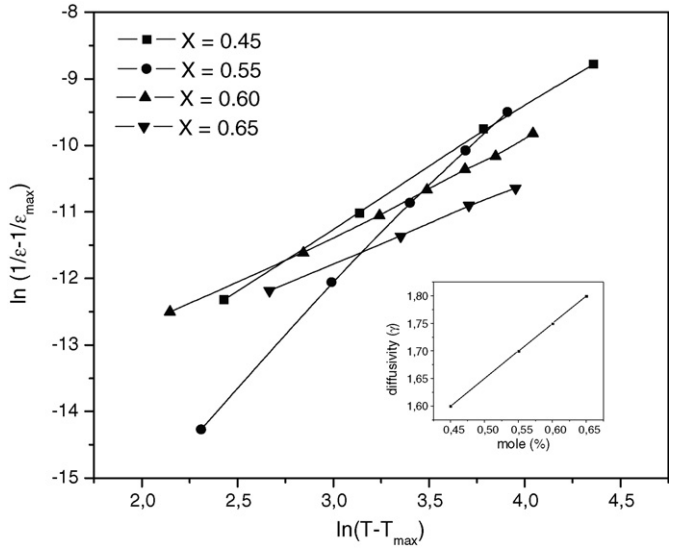

Fig. 7. Variation of $\ln(1/\varepsilon - 1/\varepsilon_{max})$ vs $\ln(T - T_{max})$ in the paraelectric region at 100 kHz.

trons on Fe^{3+} ions is caused by incorporating Pb^{2+} ions to A sites and/or Ti^{4+} ions to B sites of the perovskite structure of $BiFeO_3$. This structural distortion could lead to the suppression of the spin spiral and hence enhance the magnetization in the system.

The quantitative assessment of the diffusivity (γ) of the broadened peaks in the paraelectric phase was evaluated using the expression $\ln(1/\varepsilon - 1/\varepsilon_{max})$ vs $(T - T_c)^{\gamma}$ [27]. The plot (Fig. 7) of $\ln(1/\varepsilon - 1/\varepsilon_{max})$ vs $\ln(T - T_{max})$ for all compositions was extracted from the plot by fitting a straight-line equation. The value of γ was found to be between 1 (normal Curie Weiss behavior) and 2 (completely disordered), which further confirmed the diffuse phase transition in the materials. The double logarithmic relationship between $(1/\varepsilon - 1/\varepsilon_{max})$ and $(T - T_{max})$, unequivocally displays linear behavior in the temperature range between T_{max} and T_{cw}. The values of γ fall into $1.6 < \gamma < 1.8$. For the comparative purpose, the plots of diffusivity against concentration at 100 kHz for various compositions are shown in Fig. 7 as an inset figure. The role of BMT, increase the diffusivity of this ferroelectric systems. A maximum value of diffusivity was found at 0.65 mol% BMT.

4. Conclusions

BF–BMT–PT solid solution ceramics were prepared using solid-state reaction method. BF–BMT–PT ceramics have tetragonal crystal structure at room temperature exhibiting better homogeneity and formation of compounds. $BiFeO_3$ doping in BMT–PT exhibits many interesting feature, such as shift in transition temperature, diffuse phase transition and magnetic properties. This composition also shows a maximum diffusivity with higher degree of disorderness. The diffuseness of phase transition is appreciably increased by BMT doping. Marked non-Curie–Weiss behavior was observed, which diminished with an increase in BMT concentration. The magnetization increases with the increase in content of BF–BMT. The magnetization is higher, when the concentration of BF–BMT–PT is increased from 0.45 to 0.65. The two compositions ($X = 0.60$, 0.65) have highly dense, uniformly distributed grains with nearly no pores and hence it shows higher resistivity. Well-saturated P–E loop could be observed with increasing E for $X = 0.65$. Experiments are in progress to improve the density, dielectric and magnetic properties of the samples.

Acknowledgement

The authors are grateful to Fundação para a Ciência e a Tecnologia (FCT) Lisboa for providing financial assistance for this research grant.

References

[1] R.E. Cohen, Nature 358 (1992) 136–138.
[2] L. Bellaiche, A. Garcia, D. Vanderbilt, Phys. Rev. Lett. 84 (2000) 5427–5430.
[3] I. Grinberg, V.R. Cooper, A.M. Rappe, Nature 419 (2002) 909–911.
[4] Y. Saito, H. Takao, T. Tani, T. Nonoyama, K. Takatori, T. Homma, T. Nagaya, M. Nakamura, Nature 432 (2004) 84–87.
[5] R.E. Eitel, C.A. Randall, T.R. Shrout, P.W. Rehrig, W. Hackenberger, S.E. Park, Jpn. J. Appl. Phys. 40 (2001) 5999–6002.
[6] M.R. Suchomel, P.K. Davies, Appl. Phys. Lett. 86 (2005) 262905.
[7] Y. Uratani, T. Shishidou, F. Ishii, T. Oguchi, Jpn. J. Appl. Phys. 44 (2005) 7130–7133.
[8] M.D. Snel, W.A. Groen, G.D. With, J. Eur. Ceram. Soc. 25 (2005) 3229–3233.
[9] A. Moure, M. Algueró, L. Pardo, E. Ringgaard, A.F. Pedersen, J. Eur. Ceram. Soc. 27 (2007) 237–245.
[10] J. Wang, J.B. Neaton, H. Zheng, V. Nagarajan, S.B. Ogale, B. Liu, D. Viehland, V. Vaithyanathan, D.G. Schlom, U.V. Waghmare, N.A. Spaldin, K.M. Rabe, M. Wuttig, R. Ramesh, Science 299 (2003) 1719–1722.
[11] A.A. Belik, S. Iikubo, K. Kodama, N. Igawa, S. Shamoto, S. Niitaka, M. Azuma, Y. Shimakawa, M. Takano, F. Izumi, E.T. Muromachi, Chem. Mater. 18 (2006) 798–803.
[12] S.A. Fedulov, Y. Veneutsev, G.A. Zhdanov, E.G. Smazheuskaya, I.S. Rez, Sov. Phys. Crystallogr. 7 (1962) 62.
[13] V.A. Bokov, N.A. Grigoryan, M.F. Bryzhina, V.S. Kazaryan, Bull. Acad. Sci. USSR, Phys. Ser. (Engl. Transl.) 33 (1969) 1082.
[14] R. Eitel, C.A. Randall, T.R. Shrout, S.E. Park, Jpn. J. Appl. Phys. 41 (2002) 2099.
[15] M. Polomska, W. Kaczmarek, Z. Pajak, J. Phys. Status Solidi A 23 (1974) 567.
[16] C.A. Randall, R. Eitel, T.R. Shrout, D.I. Woodward, I.M. Reaney, J. Appl. Phys. 93 (2003) 9271.
[17] C.F. Yang, C.C. Diao, H.H. Chung, H.H. Huang, H.M. Chen, J. Alloys Compd. 461 (2008) 404–409.
[18] S. Sharma, D.A. Hall, J. Electroceram. 20 (2008) 81–87.
[19] S. Sharma, D.A. Hall, A. Sinha, Mater. Res. Bull. 44 (2009) 1405–1410.
[20] R. Rai, A. Sinha, S. Sharma, N.K.P. Sinha, J. Alloys Compd, doi:10.1016/j.jallcom.2009.06.124.
[21] E. Wu, POWD, an interactive powder diffraction data interpretation and indexing program Ver2.1 School of Physical Science Flinders University of south Australia Bedford Park S.A J042 AU.
[22] D. Damjanovic, J. Appl. Phys. 82 (1997) 1788.
[23] J. Mal, R.N.P. Choudhary, Phase Transit. 62 (1997) 19.
[24] N.K. Misra, R. Sati, R.N.P. Choudary, Mater. Lett. 24 (1995) 313.
[25] K.V. Rao, A. Smakula, J. Appl. Sci. 37 (1966) 319.
[26] C. Ederer, N.A. Spaldin, Phys. Rev. B 71 (2005) 060401(R)–060404 (R).
[27] M.S. Pilgrim, E. Sutherland Audrey, R. Winzer, J. Am. Ceram. Soc. 73 (1990) 3122.